IOP Publishing Nanotechnology
Nanotechnology 29 (2018) 395201 (6pp) https://doi.org/10.1088/1361-6528/aad0af

High performance self-gating graphene/MoS_2 diode enabled by asymmetric contacts

Muhammad Atif Khan[1], Servin Rathi[1], Changhee Lee[1], Yunseob Kim[1], Hanul Kim[2], Dongmok Whang[2], Sun Jin Yun[3], Doo-Hyeb Youn[3], Kenji Watanabe[4], Takashi Taniguchi[4] and Gil-Ho Kim[1]

[1] Department of Electronic, Electrical and Computer Engineering, School of Electronic and Electrical Engineering and Sungkyunkwan Advanced Institute of Nanotechnology (SAINT), Sungkyunkwan University, Suwon 16419, Republic of Korea
[2] School of Advanced Materials Science and Engineering and Sungkyunkwan Advanced Institute of Nanotechnology (SAINT), Sungkyunkwan University, Suwon 16419, Republic of Korea
[3] ICT Components and Materials Technology Research Division, Electronics and Telecommunications Research Institute, Daejeon 34129, Republic of Korea
[4] Advanced Materials Laboratory, National Institute for Material Science, 1-1 Namiki, Tsukuba, 305-0044, Japan

E-mail: ghkim@skku.edu

Received 11 May 2018, revised 17 June 2018
Accepted for publication 3 July 2018
Published 18 July 2018

Abstract

A graphene-MoS_2 (GM) heterostructure based diode is fabricated using asymmetric contacts to MoS_2, as well as an asymmetric top gate (ATG). The GM diode exhibits a rectification ratio of 5 from asymmetric contacts, which is improved to 10^5 after the incorporation of an ATG. This improvement is attributed to the asymmetric modulation of carrier concentration and effective Schottky barrier height (SBH) by the ATG during forward and reverse bias. This is further confirmed from the temperature dependent measurement, where a difference of 0.22 eV is observed between the effective SBH for forward and reverse bias. Moreover, the rectification ratio also depends on carrier concentration in MoS_2 and can be varied with the change in temperature as well as back gate voltage. Under laser light illumination, the device demonstrates strong opto-electric response with 100 times improvement in the relative photo current, as well as a responsivity of 1.9 A W^{-1} and a specific detectivity of 2.4×10^{10} Jones. These devices can also be implemented using other two dimensional (2D) materials and suggest a promising approach to incorporate diverse 2D materials for future nano-electronics and optoelectronics applications.

Supplementary material for this article is available online

Keywords: diode, rectification, MoS_2, graphene

(Some figures may appear in colour only in the online journal)

1. Introduction

Graphene and other two dimensional (2D) materials have recently attracted great attention in the research community for various electronics applications, as well as for fundamental science and applied physics [1, 2]. Their unique properties, like atomic scale thickness, strong gate modulation and mechanical flexibility, make them a strong candidate for future electronics [3, 4]. Moreover, atomically thin layers of different 2D materials can be stacked to form different combinations of heterostructures to achieve desired properties for various applications [5, 6]. The operation of various high performance devices, like tunneling transistors, [7] vertical transistors [8], inverters [9], diodes [10] and ambipolar transistors [11] has already been demonstrated based on 2D materials. A diode is one of the most important electronics devices with the main feature of rectifying output characteristics. Typical semiconductor diodes are mostly fabricated by selective doping techniques like diffusion or ion implantation of dopants. However, to fulfill the requirement of ultra-fast and low power modern electronics, channel size is reducing drastically, which puts severe limitations on the fabrication and doping techniques for sub-nanoscale devices. Therefore, multiple new configurations of diodes based on 2D materials have been proposed and studied. These studies include diodes fabricated using surface and plasma doping techniques [12, 13]. Liquid gates, asymmetric contacts and split gates have also been used to achieve diode operation in 2D materials [14–17]. Further, the van der Waal heterostructure of different 2D materials have also shown diode like properties. These heterostructures include BP/MoS_2 [18], MoS_2/WSe_2 [10], InAs/WSe_2 [19], and graphene/MoS_2 (GM) [20, 21]. Because of semi-metallic nature of graphene, GM heterostructure based diodes show insignificant rectification ratio [20, 21], which is one of the most important parameter to determine the performance of a diode. This is because graphene form better contact with MoS_2 as compared to high barrier metal contact and the device operates like Schottky diode due to this asymmetry in contacts. As both graphene and MoS_2 are the most attractive 2D materials due to their interesting electrical, optical and energy band characteristics, therefore improving the performance of GM diode would find wide applications in electrical and optical devices. In this work, we have fabricated a GM diode by using different contacts materials to MoS_2 flake i.e., graphene contact on one side and the metal contacts on the other side. The performance of the fabricated diode is further improved by incorporating an asymmetric top gate (ATG) to modulate the barrier height in sync with the polarity of the applied bias. After the incorporation of an ATG structure, the rectification ratio of the device increases from 5 to 10^5 and also affects the relative photo current, which shows a selective improvement of two orders of magnitude in this ATG-GM diode. The proposed configuration can also be implemented to improve the characteristics of diodes based on other 2D materials and heterostructures.

2. Results and discussions

Figure 1(a) is the schematic drawing of GM self-gating diode in which graphene contact is used on one side of MoS_2 while metal (Cr/Au) contact is used on the other side. The device is fabricated by first exfoliating MoS_2 from a commercial bulk crystal on a silicon substrate capped with 300 nm SiO_2 using the standard mechanical exfoliation method. Similarly graphene is also exfoliated and suitable flakes are selected using optical microscope and transferred on top of MoS_2 using the polymer assisted transfer technique. Electrodes pattern is made by electron beam lithography followed by metal (Cr/Au 10/30 nm) deposition in electron beam deposition chamber. Similar procedure is adopted to transfer h-BN on top of the device and the top metal gate, ATG, is deposited in such a way that it is connected with metal contact of MoS_2 as well, as illustrated in figure 1(a). Graphene and MoS_2 flakes were characterized by Raman spectroscopy using a 532 nm laser under ambient conditions as shown in figure 1(b). MoS_2 Raman spectrum comprise of signature MoS_2 peaks: E_{2g} and A_{1g} at frequencies of 383 cm^{-1} and 405 cm^{-1}, respectively [22]. The difference of peak frequencies (22 cm^{-1}) indicates that MoS_2 thickness is more than four layers, [22] which is further confirmed by atomic force microscopy (AFM) and comes out to be 4.2 nm (six layers) as shown in figure S1, available online at stacks.iop.org/NANO/29/395201/mmedia. Likewise, the Raman spectrum of graphene is comprised of signature graphene peaks G and 2D, at frequencies of 1582 cm^{-1} and 2680 cm^{-1}, respectively [23]. Graphene and h-BN thickness is also confirmed by AFM and comes out to be 1.5 nm (five layers) and 22 nm, respectively, as shown in figure S1. Further, MoS_2 channel length and width are 7 μm and 3 μm, respectively.

Figure 1(c) is the output characteristics of GM device after h-BN transfer and before the deposition of the top gate at different back gate voltages, V_{bg} and a rectification ratio of $\sim$5 can be seen in the current–voltage characteristics. This rectification is due to presence of asymmetric contacts to MoS_2 layer, as the graphene contact exhibits less contact resistance compared to metal contact because of low barrier at the GM interface [24, 25]. However, after the deposition of top gate, GM device exhibits significantly higher asymmetry (I_{on}/I_{off}) of 10^5 in the output characteristics, where I_{on} is the device current at $V_d = -2$ V and I_{off} is the device current at $V_d = 2$ V as seen from figure 1(d). This increase in the rectification ratio after the deposition of top gate can be explained with the help of schematics in figures 2(a) and (b).

Figure 2 explains the mechanism behind the asymmetric transport based on the fact that under high drain voltage, the device current is mainly affected by the barrier at injection contact (source electrode only) [26, 27]. During forward bias, as shown in figure 2(a), the injection of electrons in MoS_2 is from the graphene side, as the graphene electrode is negative while the other metal electrode is positive. The ATG will generate positive electric field to accumulate electrons in the MoS_2 near the drain electrode, thus making it highly conducting. This accumulation of electrons in MoS_2 combined with the injection of electrons from the less resistive graphene contact results in high channel current as shown in figure 2(a). During reverse bias, graphene electrode is positive while the metal electrode and ATG is negative. In this case, the injection of electrons in MoS_2 is from metal electrode, however, because of negative bias, the ATG will generate negative electric field which leads to the depletion of electrons in MoS_2. This depletion not only makes the channel more resistive but also results in increased effective Schottky barrier height (SBH) for electron injection. Although, for a particular metal and semiconductor, SBH is fixed, however, effective SBH can vary with the change in carrier concentration. This change in carrier concentration in the channel can vary the depletion width at metal–semiconductor interface which affects the injection of carriers. The carrier injection consists of three main components: thermionic emission, thermionic field emission and tunneling component, of which, the last two components vary exponentially with change in depletion width. This variation leads to an observed change in

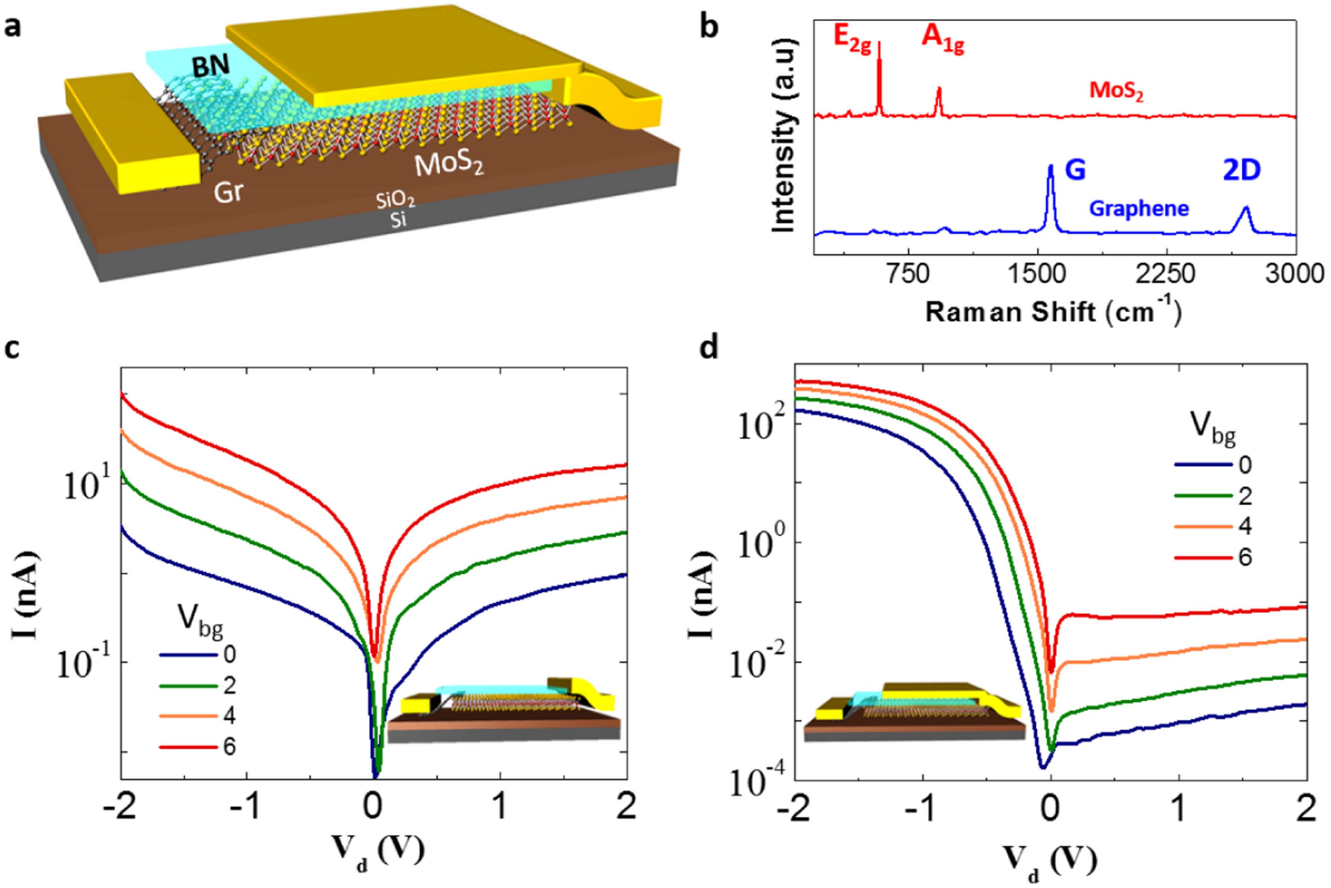

Figure 1. (a) Schematic of the GM self-gating diode, (b) Raman spectra of MoS_2 and graphene, (c) output characteristics of GM diode before the incorporation of ATG (semi-logarithmic scale), (d) output characteristics of GM diode after the deposition of ATG (semi-logarithmic scale).

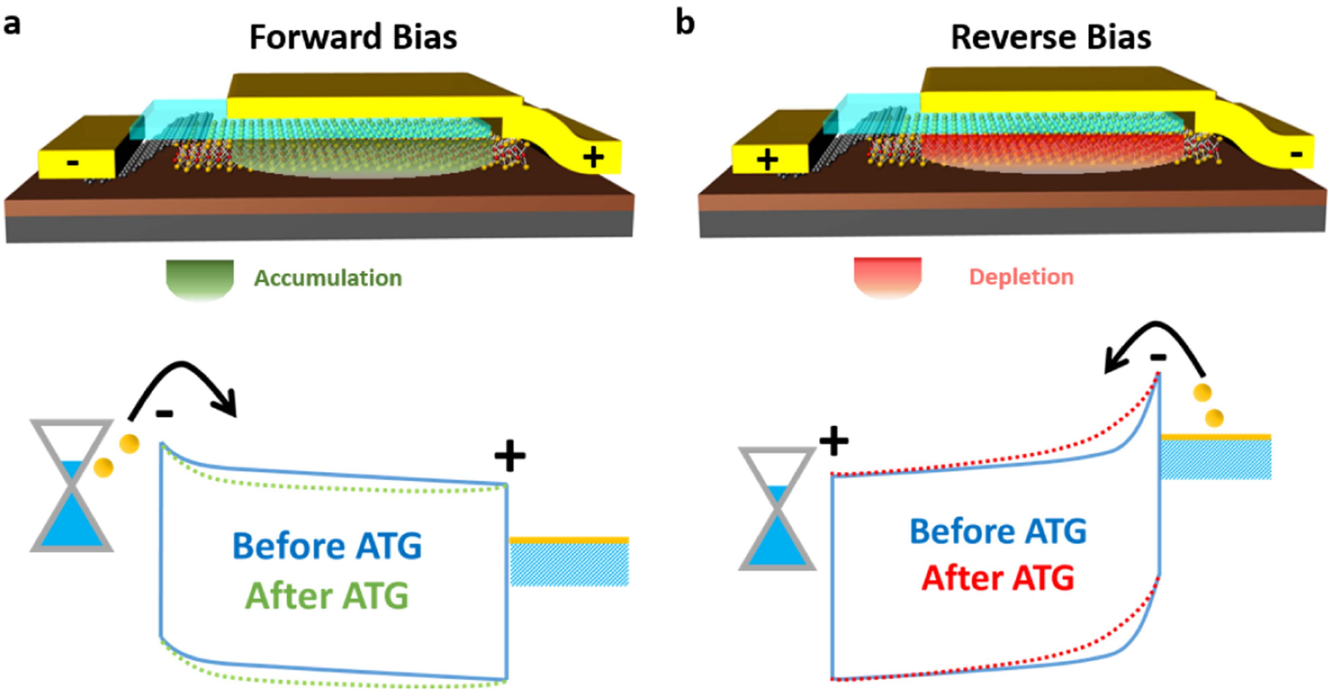

Figure 2. (a) Schematic and band diagram showing contacts polarity and electron accumulation in MoS_2 during forward bias, (b) schematic and band diagram showing contacts polarity and electron depletion in MoS_2 during reverse bias.

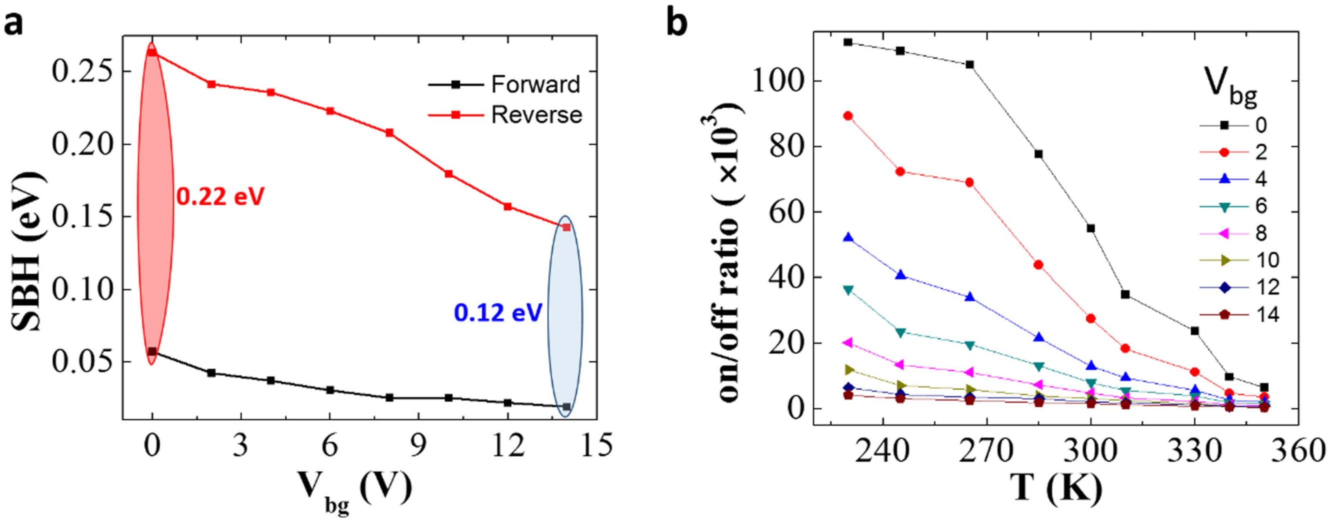

Figure 3. (a) Effective SBH obtained from temperature dependent measurement at different back gate voltages during forward and reverse bias, (b) plot between rectification ratio of device and temperature at different back gate voltages.

the measured SBH also known as effective SBH. Therefore, during reverse bias, resistive channel combined with increased effective SBH at metal–MoS_2 interface results in highly reduced channel current as seen in figure 1(d).

We have further validated this explanation of variable SBH from the temperature dependent measurement by extracting the effective SBH during forward and reverse bias. The output characteristics of the device are measured at different V_{bg}, in a temperature range of 230–350 K. Equation (1) has been used to extract the effective SBH [26, 28]:

$$I = AA^{*}T^{3/2}\ \exp\left(-\frac{q\varnothing_b}{k_B T}\right)\left(\exp\left(\frac{qV_d}{k_B T}-1\right)\right). \tag{1}$$

In this equation, I is the total current, A is the area, A^{*} is the modified Richardson constant, $\varnothing_b$ is the effective SBH, V_d is the drain voltage, q is the electron charge, k_B is Boltzmann constant and T is temperature in Kelvin. We measured the device current at different temperatures and the effective SBH is extracted from the slope of linear fit of $\ln(I/T^{3/2})$ versus $1/T$. The extracted values of effective SBH at different V_{bg} is shown in figure 3(a).

It can be seen from figure 3(a) that effective SBH for forward bias is much less than that of the reverse bias. This difference in effective SBH validates the previous explanation where rectification in the I–V characteristics has been attributed to the accumulation and depletion effect of ATG on the carrier concentration and thus the effective SBH. Another important observation in figure 3(a) is that effective SBH of forward as well as reverse bias reduces with an increase in V_{bg}. However, the rate of change for forward bias is less than that of reverse bias and therefore, the difference between the two also reduces with increasing V_{bg}. The difference in effective SBH for forward and reverse bias at $V_{bg} = 0$ V is around 0.22 eV, which reduces to around 0.12 eV at $V_{bg} = 14$ V. This is due to the fact that the increase in electron concentration in the channel with V_{bg}, cancels out the increment in the effective SBH due to ATG, therefore the effective SBH decreases at a higher rate in the reverse bias (at the metal–MoS_2 contact) as compared to forward bias (GM contact).

This trend also appears in figure 3(b), where the on/off ratio of the device substantially changes with variations in both temperature, as well as V_{bg}. The increase in either V_{bg} or temperature results in an increased electron concentration in the channel and subsequently, reduction of effective SBH. As shown in figure 3(a), an effective SBH in reverse bias is more sensitive to carrier concentration and reduces at a rate faster than that of forward bias. Therefore, the on/off ratio of the device also reduces with increasing temperature as well as V_{bg}, as seen in figure 3(b). This unique dependence of on/off ratio on the carrier concentration modulated by both ATG and back gate can also be utilized to improve the opto-electrical characteristics, where the carrier concentration is modulated by the photo-generated electron–hole carriers.

Figure 4 presents the relative photo current of device, which is an important parameter to evaluate the performance of any optical sensor. The GM device is illuminated by a light source of 655 nm and the relative photo current is obtained by first subtracting the dark current from total current under laser illumination and then dividing the difference with the dark current ($I_{ph} = I_{laser} - I_{dark}$, where I_{laser} is total current under illumination). Before deposition of top gate, as shown in figure 4(a), relative photo current is of the order of 10^3. However, after the deposition of ATG, as shown in figure 4(b), relative photo current is increased to 10^5. As the illumination of laser results in the generation of electron–hole pairs in the MoS_2, therefore, the carrier concentration in the channel increases under illumination and as discussed earlier, under high carrier concentration, the asymmetric gating effect of top gate becomes less effective. This results in high current flowing in device under reverse bias as well, which ultimately leads to higher value of relative photo current. This increase in relative photo current by 100 times in the same device after deposition of ATG, reflects the advantage of the proposed device for optoelectronics applications. Further, we have

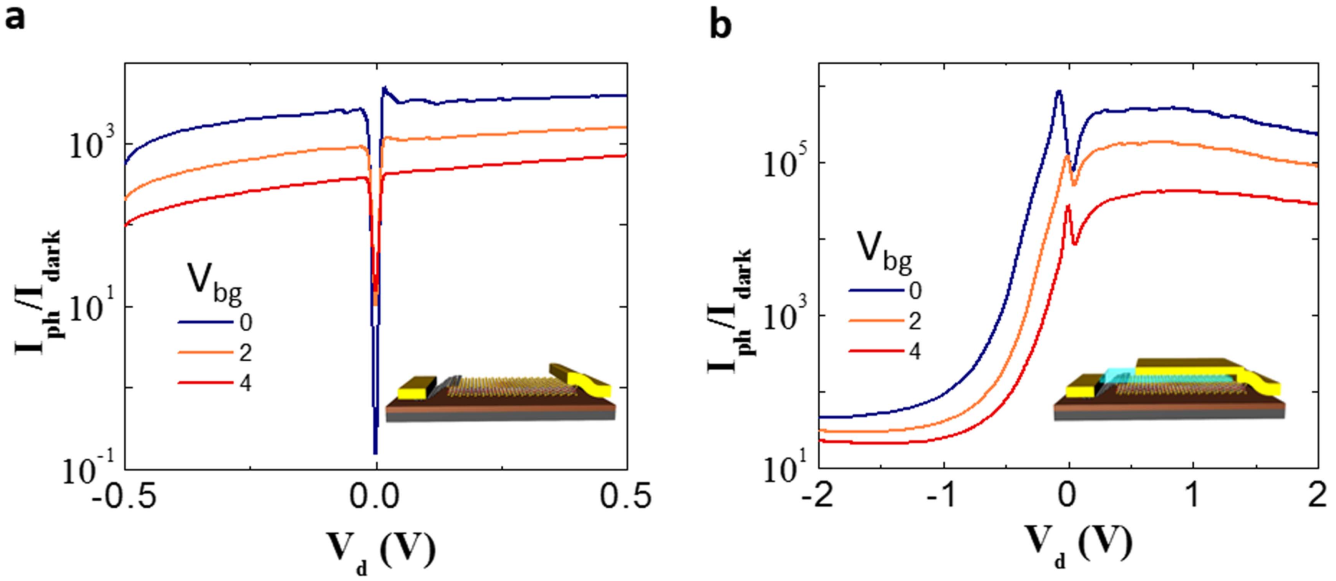

Figure 4. Plot of relative photo current and drain voltage of GM device, (a) before the deposition of ATG (b) after the deposition of ATG.

calculated the responsivity and specific detectivity of our ATG-GM device, which are the key features of any optical sensor. The maximum obtained value of responsivity is $1.90\ \mathrm{A\ W^{-1}}$ at $V_d = -2$ V, which is obtained from the ratio of the photo current to the incident laser power, $R = I_{ph}/P_{in}$ [12, 16, 20]. Specific detectivity is mostly used to determine optical sensor sensitivity and the maximum obtained value of detectivity is 2.4×10^{10} Jones, calculated by using $D^* = A^{1/2}/\mathrm{NEP}$, where A is the illuminated area and NEP is the noise equivalent power, $\mathrm{NEP} = (2qI)^{1/2}/R$.

3. Conclusions

In conclusion, we have demonstrated the operation of a doping free self-gating diode where high rectification ratio is achieved by asymmetric modulation of carrier concentration and effective SBH by the top gate. The rectification ratio of the device varies with carrier concentration in MoS_2 and can be controlled by changing temperature and back gate voltage. The ATG-GM device also evinces a strong opto-electric response, when illuminated by light source, and a 100 times improvement has been observed in relative photo current compared to the pristine GM heterostructure.

Acknowledgments

This research was supported by Basic Science Research Program through the NRF funded by the Ministry of Education, Science and Technology 2016R1A2A2A05921925, 2016R1D1A1B03932455 and Korea Research Fellowship Program through the NRF funded by the Ministry of Science and ICT (2015H1D3A1062519). This work was partly supported by Institute for Information & Communications Technology Promotion grant funded by the Korea government (MSIT) (Grant No. 2016-0-00576, Fundamental technologies of two dimensional materials and devices for the platform of new-functional smart devices). KW and TT acknowledge support from the Elemental Strategy Initiative conducted by the MEXT, Japan and the CREST (JPMJCR15F3), JST.

ORCID iDs

Gil-Ho Kim https://orcid.org/0000-0002-5153-4235

References

[1] Geim A K and Novoselov K S 2007 The rise of graphene *Nat. Mater.* **6** 183–91
[2] Wang Q H, Kalantar-Zadeh K, Kis A, Coleman J N and Strano M S 2012 Electronics and optoelectronics of two-dimensional transition metal dichalcogenides *Nat. Nanotechnol.* **7** 699–712
[3] Radisavljevic B, Radenovic A, Brivio J, Giacometti V and Kis A 2011 Single-layer MoS_2 transistors *Nat. Nanotechnol.* **6** 147–50
[4] Jariwala D, Sangwan V K, Lauhon L J, Marks T J and Hersam M C 2014 Emerging device applications for semiconducting two-dimensional transition metal dichalcogenides *ACS Nano* **8** 1102–20
[5] Pizzocchero F, Gammelgaard L, Jessen B S, Caridad J M, Wang L, Hone J, Bøggild P and Booth T J 2016 The hot pick-up technique for batch assembly of van der Waals heterostructures *Nat. Commun.* **7** 11894
[6] Geim A K and Grigorieva I V 2013 van der Waals heterostructures *Nature* **499** 419–25
[7] Britnell L *et al* 2012 Field-effect tunneling transistor based on vertical graphene heterostructures *Science* **335** 947–50
[8] Georgiou T *et al* 2012 Vertical field-effect transistor based on graphene–WS_2 heterostructures for flexible and transparent electronics *Nat. Nanotechnol.* **8** 100–3
[9] Wang H, Yu L, Lee Y-H, Shi Y, Hsu A, Chin M L, Li L-J, Dubey M, Kong J and Palacios T 2012 Integrated circuits based on bilayer MoS(2) transistors *Nano Lett.* **12** 4674–80

[10] Lee C H *et al* 2014 Atomically thin p–n junctions with van der Waals heterointerfaces *Nat. Nanotechnol.* **9** 676–81
[11] Lee I *et al* 2016 Gate-tunable hole and electron carrier transport in atomically thin dual-channel WSe_2/MoS_2 heterostructure for ambipolar field-effect transistors *Adv. Mater.* **28** 9519–25
[12] Choi M S, Qu D, Lee D, Liu X, Watanabe K, Taniguchi T and Yoo W J 2014 Lateral MoS_2 p–n junction formed by chemical doping for use in high-performance optoelectronics *ACS Nano* **8** 9332–40
[13] Chen M, Nam H, Wi S, Ji L, Ren X, Bian L, Lu S and Liang X 2013 Stable few-layer MoS_2 rectifying diodes formed by plasma-assisted doping *Appl. Phys. Lett.* **103** 142110
[14] Khan M A, Rathi S, Park J, Lim D, Lee Y, Yun S J, Youn D H and Kim G H 2017 Junctionless diode enabled by self-bias effect of ion gel in single-layer MoS_2 device *ACS Appl. Mater. Interfaces* **9** 26983–9
[15] Zhang Y J, Ye J T, Yomogida Y, Takenobu T and Iwasa Y 2013 Formation of a stable p–n junction in a liquid-gated MoS_2 ambipolar transistor *Nano Lett.* **13** 3023–8
[16] Khan M A, Rathi S, Lee I, Li L, Lim D, Kang M and Kim G-H 2016 P-doping and efficient carrier injection induced by graphene oxide for high performing WSe_2 rectification devices *Appl. Phys. Lett.* **108** 093104
[17] Ross J S *et al* 2014 Electrically tunable excitonic light-emitting diodes based on monolayer WSe_2 p–n junctions *Nat. Nanotechnol.* **9** 268–72
[18] Deng Y, Luo Z, Conrad N J, Liu H, Gong Y, Najmaei S, Ajayan P M, Lou J, Xu X and Ye P D 2014 Black phosphorus-monolayer MoS_2 van der Waals heterojunction p–n diode *ACS Nano* **8** 8292–9
[19] Chuang S, Kapadia R, Fang H, Chia Chang T, Yen W C, Chueh Y L and Javey A 2013 Near-ideal electrical properties of $InAs/WSe_2$ van der Waals heterojunction diodes *Appl. Phys. Lett.* **102** 2–6
[20] Rathi S *et al* 2015 Tunable electrical and optical characteristics in monolayer graphene and few-layer MoS_2 heterostructure devices *Nano Lett.* **15** 5017–24
[21] Kwak J Y, Hwang J, Calderon B, Alsalman H, Munoz N, Schutter B and Spencer M G 2014 Electrical characteristics of multilayer MoS_2 FET's with MoS_2/graphene heterojunction contacts *Nano Lett.* **14** 4511–6
[22] Lee C, Yan H, Brus L E, Heinz T F, Hone J and Ryu S 2010 Anomalous lattice vibrations of single-and few-layer MoS_2 *ACS Nano* **4** 2695–700
[23] Ferrari A C *et al* 2006 Raman spectrum of graphene and graphene layers *Phys. Rev. Lett.* **97** 187401
[24] Cui X *et al* 2015 Multi-terminal transport measurements of MoS_2 using a van der Waals heterostructure device platform *Nat. Nanotechnol.* **10** 534–40
[25] Yu L *et al* 2014 Graphene/MoS_2 hybrid technology for large-scale two-dimensional electronics *Nano Lett.* **14** 3055–63
[26] Kim C, Moon I, Lee D, Choi M S, Ahmed F, Nam S, Cho Y, Shin H J, Park S and Yoo W J 2017 Fermi level pinning at electrical metal contacts of monolayer molybdenum dichalcogenides *ACS Nano* **11** 1588–96
[27] Ahmed F, Choi M S, Liu X and Yoo W J 2015 Carrier transport at the metal–MoS_2 interface *Nanoscale* **7** 9222–8
[28] Anwar A, Nabet B, Culp J and Castro F 1999 Effects of electron confinement on thermionic emission current in a modulation doped heterostructure *J. Appl. Phys.* **85** 2663–6